Raman Tensor of Layered Black Phosphorous

Yanming Zhu
Sun Yat-sen University
Wei Zheng (zhengw37@mail.sysu.edu.cn)
Sun Yat-Sen University https://orcid.org/0000-0003-4329-0469
Weiliang Wang
Sun Yat-Sen University
Siqi Zhu
Sun Yat-Sen University
Linxuan Li
Sun Yat-Sen University
Lu Cheng
Sun Yat-Sen University
Mingge Jin
Sun Yat-Sen University
Ying Ding
Sun Yat-sen University
Feng Huang
Sun Yat-Sen University

Research

Keywords: Black phosphorous, polarized Raman spectrum, differential polarizability, Raman tensor

Posted Date: April 7th, 2020

DOI: https://doi.org/10.21203/rs.3.rs-20864/v1

Version of Record: A version of this preprint was published on July 20th, 2020. See the published version at https://doi.org/10.1186/s43074-020-00017-7.

Raman Tensor of Layered Black Phosphorous

Yanming Zhu, Wei Zheng*, Weiliang Wang, Siqi Zhu, Linxuan Li, Lu Cheng, Mingge Jin, Ying Ding and Feng Huang

State Key Laboratory of Optoelectronic Materials and Technologies, School of Materials, Sun Yat-sen University, Guangzhou, Guangdong, 510275, China.

Corresponding author: zhengw37@mail.sysu.edu.cn

Abstract： Black phosphorous is an orthorhombic with a strong Raman anisotropy in the basal and cross plane. However, up to now, almost all the studies on anisotropy of black phosphorous have focused on basal plane but neglected cross plane. Here, we performed a systematic angle-resolved polarized Raman scattering on the basal and cross plane of black phosphorous and obtained its integral Raman tensors. In addition, we discovered that Raman intensity ratio (I_{xx}: I_{yy}:I_{zz}) of A_g^1 mode is 256:1:5 when the polarization direction of incident light is along different crystal axes. According to first-principle calculated results, we confirmed that the strong Raman anisotropy is due to larger differential polarizability of A_g^1 mode along *a*-axis. This phenomenon is also observed in the A_g^2 mode.

Keywords: Black phosphorous, polarized Raman spectrum, differential polarizability, Raman tensor

1. Introduction

Recently, much attention has been focused on directional selective optoelectronic devices [1-5], of which the high directional charge and energy transfer characteristic are important indictors to evaluate performance of devices. The directional selective characteristic of optoelectronic device originates from anisotropy of atomic arrangement. Based on group theory, black phosphorous (BP) belongs to D_{2h} space group, which suggests that BP has different atomic arrangements along zigzag and armchair directions [6-9]. Therefore, BP is one of the excellent candidates to fabricate directional selective optoelectronic devices.

Raman polarization characteristic, as an important branch of anisotropy, is determined by Raman tensor, which is a key index to evaluate Raman scattering intensity [10-12]. In order to obtain integral Raman tensor, Angle-resolved polarized Raman (APR) spectroscopy as a powerful and undamaged tool was performed, which has been used in our previous work where we studied the Raman polarization characteristic of traditional anisotropic crystal, such as AlN, GaN and ZnO [13-16]. BP, as an anisotropic layered material, have attracted much attention in the aspects of optical and electrical polarization characteristics. However, almost all the studies on the anisotropy of BP put focus on basal plane rather than cross plane so far [17-23], which causes a lack of integral Raman tensor. This blank can be filled by studying the anisotropy of cross plane.

In this work, we systematically analyzed the APR spectra of cross and basal planes of BP and discovered that A_g^1 and A_g^2 modes have strong Raman anisotropies along different crystal axes. Raman scattering intensity ratio of A_g^1 mode along different

crystal axes (I_{xx}: I_{yy}:I_{zz}) is up to 256:1:5, and that of A_g^2 mode is 10:1:5. According to first-principle calculation, we confirmed the strong Raman anisotropies of A_g^1 and A_g^2 modes originate from the difference of differential polarizability along different crystal axes.

2. Method

Here, we measured APR spectrum of BP via backscattering geometry Renishaw spectrometer (inVia Reflex), where 488 nm laser was equipped as excitation light and focused on the basal or cross plane through $50\times$ long focus quartz lens. The polarization direction of incident light is fixed, and to ensure only the scattering light with the same polarization direction as incident light was collected, a polarizer was placed and fixed in the detection light path. During the experimental process, layered BP sample was rotated in the step of 10°. Besides, to prevent sample from being damaged due to overheating, laser power density and acquisition time were set as 5 mW and 1s. In addition, integration number is set as 10 times to reduce signal-to-noise ratio (SNR). In experiment, measured BP sample is a single crystal with the size of 2 mm, and the orientations of crystal axes are shown in Fig. 1a and 1b, where the basal and cross plane are corresponding to (010) and (100) plane respectively.

3. Results and discussion

Two representative Raman spectra are presented in Fig. 1c and 1d, corresponding to basal and cross plane. When incident light propagates along *b*-axis [010], the

collected APR spectra of the three modes (A_g^1 (363 cm^{-1}), A_g^2 (470 cm^{-1}) and B_{2g} (434 cm^{-1})) exhibit period changes. Similarly, when incident light propagates along *a*-axis [100], the collected APR spectra of the three modes (A_g^1, A_g^2 and B_{3g}^1 (436 cm^{-1})) also exhibit period changes. And the periods of A_g^1 and A_g^2 are 180° and those of B_{3g}^1 and B_{2g} are 90°. According to Raman selection rule, when the polarization direction of excitation light is same as that of collected scattering light, B_{2g} mode is forbidden in the Raman scattering process of cross plane, and B_{3g}^1 mode cannot be observed during the Raman scattering process of basal plane. Therefore, B_{2g} and B_{3g}^1 modes can be used as criteria to distinguish crystal plane.

Based on the APR spectra of basal and cross plane, we obtained Raman scattering intensity of each mode when the polarization direction of incident light is along different crystal axes. As shown in Fig. 2b, 2d, 2f and 2h, when incident light propagates along *b*-axis, the Raman scattering intensity ratio (I_{xx}: I_{zz}) of A_g^1 mode is 11.1, and that of A_g^2 mode is 1.94. When incident light propagates along *a*-axis, the Raman scattering intensity ratio (I_{zz}: I_{yy}) of A_g^1 mode is 23.1 and that of A_g^2 mode is 4.9. Combining with the APR spectra of basal and cross plane, the Raman scattering intensity ratios of A_g^1 and A_g^2 modes along different crystal axes that are 256:1:23 and 9.6:1:4.9 can be obtained. It is obvious that there are strong Raman anisotropies of A_g^1 and A_g^2 modes along different crystal axes, which can be elaborated with Raman selection rule and the definition of Raman scattering intensity [17, 18].

Specifically, according to classical Raman scattering theory, Raman scattering intensity *I* for Raman active mode is given by [10]

$$I \sim |\boldsymbol{e_s R e_i}|^2, \tag{1}$$

where $\boldsymbol{e_i}$ and $\boldsymbol{e_s}$ represent the polarization direction vectors of incident and scattering light respectively. To explore the polarization characteristic of BP, $\boldsymbol{e_i}$ is parallel to $\boldsymbol{e_s}$ throughout the whole measurement. $\boldsymbol{R}$ denotes Raman tensor can be represented by a 3×3 matrix. According to Group theory, the Raman tensors of A_g^1, A_g^2, B_{2g} and B_{3g}^1 modes can be written as [10, 18]

$$R_{A_g^1} = \begin{pmatrix} a_1 e^{i\phi_{a_1}} & 0 & 0 \\ 0 & b_1 e^{i\phi_{b_1}} & 0 \\ 0 & 0 & c_1 e^{i\phi_{c_1}} \end{pmatrix},$$

$$R_{A_g^2} = \begin{pmatrix} a_2 e^{i\phi_{a_2}} & 0 & 0 \\ 0 & b_2 e^{i\phi_{b_2}} & 0 \\ 0 & 0 & c_2 e^{i\phi_{c_2}} \end{pmatrix},$$

$$R_{B_{2g}} = \begin{pmatrix} 0 & 0 & d \\ 0 & 0 & 0 \\ d & 0 & 0 \end{pmatrix},$$

$$R_{B_{3g}^1} = \begin{pmatrix} 0 & 0 & 0 \\ 0 & 0 & f \\ f & 0 & 0 \end{pmatrix}, \tag{2}$$

where a, b, c, d *and* f represent amplitudes of Raman tensor element, ϕ (ϕ_{a_1}, ϕ_{a_2}, ϕ_{b_1}, ϕ_{b_2}, ϕ_{c_1} and ϕ_{c_2}) is phase angle of Raman tensor element.

For $\boldsymbol{k_i}//b$, the polarization direction vectors of incident and scattering light can be written as

$$\boldsymbol{e_i} = \begin{pmatrix} sin\theta \\ 0 \\ cos\theta \end{pmatrix}, \quad \boldsymbol{e_s} = \begin{pmatrix} sin\theta \\ 0 \\ cos\theta \end{pmatrix}, \tag{3}$$

where θ denotes the angle between the a-axis of BP and the polarization direction of incident (scattering) light. Based on Eq. (1), the Raman scattering intensity expressions of A_g^1, A_g^2 and B_{2g} modes are given by

$$I_{A_g^1} \sim c_1^2 cos^4\theta + a_1^2 sin^4\theta + 2a_1 c_1 cos^2\theta sin^2\theta \cos\, \phi_{a_1 c_1},$$

$$I_{A_g^2} \sim c_2^2 cos^4\theta + a_2^2 sin^4\theta + 2a_2c_2 cos^2\theta sin^2\theta \cos\ \phi_{a_2c_2},$$

$$I_{B_{2g}} \sim d^2 sin^2 2\theta, \tag{4}$$

where $\phi_{a_1c_1}(=\phi_{a_1}-\phi_{c_1})$ and $\phi_{a_2c_2}(=\phi_{a_2}-\phi_{c_2})$ represent Raman phase differences between Raman tensor elements *a* and *c*.

For $\boldsymbol{k_i}//a$, the polarization direction vectors of incident and scattering light can be written as

$$\boldsymbol{e_i} = \begin{pmatrix} 0 \\ cos\varphi \\ sin\varphi \end{pmatrix}, \quad \boldsymbol{e_s} = \begin{pmatrix} 0 \\ cos\varphi \\ sin\varphi \end{pmatrix}, \tag{5}$$

where φ represents the angle between the *b* axis of BP and the polarization direction of incident light. Based on Eq. (1), the Raman scattering intensity expressions of A_g^1, A_g^2 and B_{3g}^1 modes can be written as

$$I_{A_g^1} \sim b_1^2 cos^4\varphi + c_1^2 sin^4\varphi + 2b_1c_1 cos^2\varphi sin^2\varphi \cos\ \phi_{b_1c_1},$$

$$I_{A_g^2} \sim b_2^2 cos^4\varphi + c_2^2 sin^4\varphi + 2b_2c_2 cos^2\varphi sin^2\varphi \cos\ \phi_{b_2c_2},$$

$$I_{B_{3g}^1} \sim f^2 sin^2 2\varphi, \tag{6}$$

where $\phi_{b_1c_1}(=\phi_{b_1}-\phi_{c_1})$ and $\phi_{b_2c_2}(=\phi_{b_2}-\phi_{c_2})$ represent Raman phase differences between Raman tensor elements *b* and *c*.

Based on the definition of Raman scattering intensity, the intensities of A_g^1, A_g^2, B_{2g} and B_{3g}^1 modes satisfy the variation of Eq. (4) and Eq. (6) with the change of rotation angle. By fitting the APR spectra of A_g^1, A_g^2, B_{2g} and B_{3g}^1 modes according to Eq. (4) and (6), the ratio relationship of amplitudes of Raman tensor elements can be obtained, as shown in Table I. For A_g^1 mode, the ratio of Raman tensor elements amplitudes a_1 to c_1 is 3.33, and that of c_1 to b_1 is 4.8. Consequently, Raman tensor elements amplitudes including a_1, b_1 and c_1 satisfies the relationship of

$a_1 > c_1 > b_1$. Similarly, for A_g^2 mode, its diagonal Raman tensor elements amplitudes also satisfies the relationship of $a_2 > c_2 > b_2$.

By the definition of Raman tensor element, Raman tensor element R_{ij}^q is given by the derivative of susceptibility χ_{ij} with regard to atom position [10], thus

$$R_{ij}^q = V_{prim} \sum_{\mu=1}^{N} \sum_{l=1}^{3} \frac{\partial \chi_{ij}}{\partial r_l(\mu)} \frac{e_l^q(\mu)}{\sqrt{M_\mu}}, \tag{7}$$

where M_μ and V_{prim} represent the atomic mass of μth atom and volume of unit cell respectively; $r_l(\mu)$ is the position of μth atom along the direction *l* and $e_l^q(\mu)$ is the eigenvector of qth phonon of μth atom. Due to linear relationship between polarizability α_{ij} and susceptibility χ_{ij} $\left(\alpha_{ij} = \varepsilon_0 \chi_{ij}\right)$, Raman tensor element R_{ij}^q can also be written as

$$R_{ij}^q = V_{prim} \sum_{\mu=1}^{N} \sum_{l=1}^{3} \frac{\partial \alpha_{ij}}{\partial r_l(\mu)} \frac{e_l^q(\mu)}{\varepsilon_0 \sqrt{M_\mu}}. \tag{8}$$

where $\partial \alpha_{ij} / \partial r_l(\mu)$ can be defined as the differential polarizability with Raman scattering intensity directly reflected. For A_g^1 mode, when incident light propagates along *b*-axis, the differential polarizability along *a*-axis is larger than that along *c*-axis, determining a larger Raman scattering intensity when the polarization direction of incident light is parallel to *a*-axis.

In addition, the susceptibility χ_{ij} is also related to relative permittivity ε_{ij} $(\chi_{ij} = \varepsilon_{ij} - 1)$. Thus, Raman tensor element can be transformed into

$$R_{ij}^q = V_{prim} \sum_{\mu=1}^{N} \sum_{l=1}^{3} \frac{\partial \varepsilon_{ij}}{\partial r_l(\mu)} \frac{e_l^q(\mu)}{\sqrt{M_\mu}}. \tag{9}$$

More importantly, the relative permittivity ε_{ij} can be calculated by first-principle. The Raman tensors of A_g^1 and A_g^2 modes can be obtained by calculating the change of relative permittivity before and after corresponding vibration. Here, we calculated the

Raman tensors of various vibration modes via Vienna Ab-initio Simulation Package (VASP) [24-35] and open source package Phonopy. During the density functional perturbation theory (DFPT) calculation, a $3 \times 3 \times 3$ supercell was adopted to obtain the force constants. A projector augmented wave (PAW) basis set with $500\ eV$ cutoff was used to expand the electronic wave functions, and Perdew-Burke-Ernzerhof functional was used as pseudopotentials. The relaxation of electron will be stopped until the free energy change between two steps is smaller than $10^{-8}\ eV$, and a high-density k-mesh of $50 \times 1 \times 50$ was performed for self-consistent calculation to obtain inductance coefficient tensors, which were shown in Table I. For A_g^1 mode, the calculated Raman tensor elements amplitudes ratio of a_1 to c_1 is 1.94, and that of c_1 to b_1 is 1.32. Therefore, a_1, b_1 and c_1 satisfy the relationship of $a_1 > c_1 > b_1$, which is consistent with experimental result. Similarly, the relationship between Raman tensor elements amplitudes a_2, b_2 and c_2 also satisfy $a_2 > c_2 > b_2$. Based on first-principle calculation, the strong Raman anisotropies of A_g^1 and A_g^2 modes are from different differential polarizabilities along different crystal axes.

Besides, the phase angle of Raman tensor element can also be calculated via first-principle. As we elaborated above, Raman tensor element is proportional to the derivative of the relative permittivity ε_{ij} with respect to spatial position of atoms. However, relative permittivity ε_{ij} is usually composed of a real part ε_{ij}' and an imaginary part ε_{ij}'', making Raman tensor element be divided into real and imaginary parts. Thus, the expression of Raman tensor element can be written as

$$R_{ij}^q = V_{prim} \sum_{\mu=1}^{N} \sum_{l=1}^{3} \frac{\partial(\varepsilon_{ij}' + i\varepsilon_{ij}'')}{\partial r_l(\mu)} \frac{e_l^q(\mu)}{\sqrt{M_\mu}}. \quad (10)$$

Calculated results are shown in Table I, where the Raman phase differences ($\phi_{a_1c_1}$, $\phi_{b_1c_1}$, $\phi_{a_2c_2}$, $\phi_{b_2c_2}$) of A_g^1 and A_g^2 are 0.23π, 0.03π, 0.01π, 0.26π respectively.

By fitting the APR spectra of A_g^1 and A_g^2 modes based on Eq. (4) and Eq. (6), the phase angels can also be obtained. When incident light spreads along *b*-axis, the Raman phase differences of A_g^1 and A_g^2 modes are 0.23π and 0.44π. When incident light propagates along the *a*-axis, the Raman phase differences of A_g^1 and A_g^2 modes are 0 and 0.28π. Compared to the calculated $\phi_{a_2c_2}$, the experimental $\phi_{a_2c_2}$ is much larger, which have puzzled us for a long time. In the Raman scattering process, except for Raman tensor, test environment and the property of materials will also affect the Raman scattering intensity. It seems difficult to find an acceptable reason to explain the large difference between experimental and theoretical values of $\phi_{a_2c_2}$.

Recently, a birefringence theory [36, 37] has been proposed to elaborate the Raman phase difference in transparent crystal, which was confirmed in the materials such as AlN, GaN [14, 38, 39]. It is generally believed that due to a nearly negligible penetration depth, the theory is invalid in narrow bandgap materials. However, this understanding may be incomplete. For opaque optical crystals, the birefringence effect may also have a significant modulation effect on Raman phase difference. According to the definition of Raman scattering intensity and the deduction in Supporting Information, a phase factor $\boldsymbol{\phi}$ and a constant $\boldsymbol{w}$ could be introduced into the Raman scattering intensity expression of A_g^2 mode in Eq. (4). Thus, when incident light propagates along *b*-axis, Raman scattering intensity of A_g^2 mode can be written as

$$I_{A_g^2} \sim c_2^2 cos^4\varphi + a_2^2 sin^4\varphi + 2a_2c_2 \cdot \boldsymbol{w} \cdot cos^2\varphi sin^2\varphi \cos\left(\phi_{a_2} - \phi_{c_2} - \boldsymbol{\phi}\right), \quad (11)$$

where $\boldsymbol{\phi}$ and $\boldsymbol{w}$ are functions respect to refractivity and extinction coefficient, given by

$$\boldsymbol{\phi} = arctg\left(\frac{n_{xr}n_{zi}-n_{xi}n_{zr}}{n_{xi}n_{zr}+n_{xr}n_{zi}}\right), \tag{12}$$

$$\boldsymbol{w} = \frac{\frac{n_{xr}n_{zi}-n_{xi}n_{zr}}{(n_{xi}^2+n_{xr}^2)(n_{zi}^2+n_{zr}^2)}}{sin\phi}, \tag{13}$$

where n_{xr} and n_{zr} denote refractive index along *x* and *z* direction respectively, and n_{xi} and n_{zi} are extinction coefficient along *x* and *z* direction respectively. Considering the birefringence effect, the theoretical value of Raman phase difference $\phi_{a_2c_2}$ of A_g^2 mode is 83°, which is close to experimental Raman phase difference 79°. Although BP is an opaque material relative to 488 nm and its penetration depth is very small, the effect of birefringence on the modulation of Raman phase difference cannot be ignored.

4. Conclusions

In this work, we analyzed APR spectra of basal and cross plane of BP systematically, and obtained complete Raman tensors. In addition, we discovered strong Raman anisotropies of A_g^1 and A_g^2 modes along different crystal axes. Via first-principle calculation, we confirmed that the strong anisotropy originates from the different differential polarizability along different crystal axes. Besides, when incident light propagates along *b*-axis, the calculated Raman phase difference of A_g^2 mode is different from the experimental value, which may be owing to the modulation of birefringence effect.

Availability of data and materials

The datasets used and analysed during the current study are available from the corresponding author on reasonable request.

Competing interests

All financial and non-financial competing interests must be declared in this section.

Funding

The financial support of this work is from the National Natural Science Foundation of China (Nos. 91333207, 61427901, 61604178, 91833301 and U1505252).

Authors' contributions

Yanming Zhu designed the experimental details and performed calculations. Siqi Zhu, Linxuan Li, Lu Cheng, Mingge Jin, Ying Ding performed the experiments. Weiliang Wang, Wei Zheng and Feng Huang directed the program.

Acknowledgements

We thank the language editing from Miss Yang.

Reference

1. Chen Y, Chen C, Kealhofer R, Liu H, Yuan Z, Jiang L, Suh J, Park J, Ko C, Choe HS, Avila J, Zhong M, Wei Z, Li J, Li S, Gao H, Liu Y, Analytis J, Xia Q, Asensio MC, Wu J. Black Arsenic: A Layered Semiconductor with Extreme In-Plane Anisotropy. Adv Mater. 2018;30:1800754
2. Chenet DA, Aslan OB, Huang PY, Fan C, van der Zande AM, Heinz TF, Hone JC. In-Plane Anisotropy in Mono- and Few-Layer ReS_2 Probed by Raman Spectroscopy and Scanning Transmission Electron Microscopy. Nano Lett. 2015;15:5667-5672
3. Yao Y, Zhang Y, Xiong W, Wang Z, Sendeku MG, Li N, Wang J, Huang W, Wang F, Zhan X, Yuan S, Jiang C, Xia C, He J. Growth and Raman Scattering Investigation of a New 2D MOX Material: YbOCl. Adv Funct Mater. 2019;29:1903017
4. Zhong X, Lee K, Meggiolaro D, Dismukes AH, Choi B, Wang F, Nuckolls C, Paley DW, Batail P, De Angelis F, Roy X, Zhu X-Y. $Mo_6S_3Br_6$: An Anisotropic 2D Superatomic Semiconductor. Adv Funct Mater. 2019;29:1902951
5. Huang S, Tatsumi Y, Ling X, Guo H, Wang Z, Watson G, Puretzky AA, Geohegan DB, Kong J, Li J, Yang T, Saito R, Dresselhaus MS. In-Plane Optical Anisotropy of Layered Gallium Telluride. ACS Nano. 2016;10:8964-8972
6. Khandelwal A, Mani K, Karigerasi MH, Lahiri I. Phosphorene – The two-dimensional black phosphorous: Properties, synthesis and applications. Mater Sci Eng B. 2017;221:17-34

7. Gupta A, Sakthivel T, Seal S. Recent development in 2D materials beyond graphene. Prog Mater Sci. 2015;73:44-126

8. Li L, Yu Y, Ye GJ, Ge Q, Ou X, Wu H, Feng D, Chen XH, Zhang Y. Black phosphorus field-effect transistors. Nat Nanotechnol. 2014;9:372

9. Tran V, Soklaski R, Liang Y, Yang L. Layer-controlled band gap and anisotropic excitons in few-layer black phosphorus. Phys Rev B. 2014;89:235319

10. Cardona M. Resonance phenomena. In: *Light Scattering in Solids II: Basic Concepts and Instrumentation* (eds Cardona M, Güntherodt G). Springer Berlin Heidelberg (1982).

11. Loudon R. The Raman effect in crystals. Adv Phys. 2001;50:813-864

12. Raman CV. A new radiation. Indian J Phys. 1928;2:387-398

13. Zheng W, Zheng RS, Wu HL, Li FD. Strongly anisotropic behavior of A1(TO) phonon mode in bulk AlN. J Alloy Compd. 2014;584:374-376

14. Zheng W, Zheng R, Huang F, Wu H, Li F. Raman tensor of AlN bulk single crystal. Photon Res. 2015;3:38-43

15. Zheng W, Yan J, Li F, Huang F. Elucidation of "phase difference" in Raman tensor formalism. Photon Res. 2018;6:709-712

16. Zheng W, Zhu Y, Li F, Huang F. Raman spectroscopy regulation in van der Waals crystals. Photon Res. 2018;6:991-995

17. Ribeiro HB, Pimenta MA, de Matos CJS, Moreira RL, Rodin AS, Zapata JD, de Souza EAT, Castro Neto AH. Unusual Angular Dependence of the Raman Response in Black Phosphorus. ACS Nano. 2015;9:4270-4276

18. Ribeiro HB, Pimenta MA, de Matos CJS. Raman spectroscopy in black phosphorus. J Raman Spectrosc. 2018;49:76-90

19. Wang T, Liu J, Xu B, Wang R, Yuan P, Han M, Xu S, Xie Y, Wu Y, Wang X. Identifying the Crystalline Orientation of Black Phosphorus by Using Optothermal Raman Spectroscopy. ChemPhysChem. 2017;18:2828-2834

20. Wu J, Mao N, Xie L, Xu H, Zhang J. Identifying the Crystalline Orientation of Black Phosphorus Using Angle-Resolved Polarized Raman Spectroscopy. Angew Chem. 2015;127:2396-2399

21. Ling X, Huang S, Hasdeo EH, Liang L, Parkin WM, Tatsumi Y, Nugraha ART, Puretzky AA, Das PM, Sumpter BG, Geohegan DB, Kong J, Saito R, Drndic M, Meunier V, Dresselhaus MS. Anisotropic Electron-Photon and Electron-Phonon Interactions in Black Phosphorus. Nano Lett. 2016;16:2260-2267

22. Mao N, Wu J, Han B, Lin J, Tong L, Zhang J. Birefringence-Directed Raman Selection Rules in 2D Black Phosphorus Crystals. Small. 2016;12:2627-2633

23. Ribeiro HB, Villegas CEP, Bahamon DA, Muraca D, Castro Neto AH, de Souza EAT, Rocha AR, Pimenta MA, de Matos CJS. Edge phonons in black phosphorus. Nat Commun. 2016;7:12191

24. Tóbik J, Tosatti E. Raman tensor calculation for magnesium phthalocyanine. Surf Sci. 2006;600:3995-3998

25. Zvereva EE, Shagidullin AR, Katsyuba SA. Ab Initio and DFT Predictions of Infrared Intensities and Raman Activities. J Phys Chem A. 2011;115:63-69

26. Saboori S, Deng Z, Li Z, Wang W, She J. β-As Monolayer: Vibrational

Properties and Raman Spectra. ACS Omega. 2019;4:10171-10175

27. Gert Irmer CR, Cameliu Himcinschi, and Jens Kortus. Raman tensor elements and Faust-Henry coefficients of wurtzite-type α-GaN: How to overcome the dilemma of the sign of Faust-Henry coefficients in α-GaN? J Appl Phys. 2014;116:245702

28. Blöchl P. Projector Agmented-Wave Method. Phys Rev B. 1994;50:17953-17979

29. Hohenberg P, Kohn W. Inhomogeneous Electron Gas. Phys Rev. 1964;136:B864

30. J. Kresse G, Joubert D. From Ultrasoft Pseudopotentials to the Projector Augmented-Wave Method. Phys Rev B. 1999;59:1758

31. Kohn W, Sham LJ. Self-Consistent Equations Including Exchange and Correlation Effects. Phys Rev. 1965;140:A1133-A1138

32. Kresse G, Furthmuller J. Efficient iterative schemes for ab initio total-energy calculations using a plane-wave basis set. Phys Rev B. 1996;54:11169-11186

33. Kresse G, Furthmüller J. Efficiency of ab-initio total energy calculations for metals and semiconductors using a plane-wave basis set. Comp Mater Sci. 1996;6:15-50

34. Monkhorst HJ, Pack JD. On Special Points for Brillouin Zone Integrations. Phys Rev B. 1976;13:5188-5192

35. P. Perdew J, Burke K, Ernzerhof M. Generalized Gradient Approximation Made Simple. Phys Rev Lett. 1996;77:3865-3868

36. Kranert C, Sturm C, Schmidt-Grund R, Grundmann M. Raman Tensor Formalism for Optically Anisotropic Crystals. Phys Rev Lett. 2016;116:127401

37. Kranert C, Sturm C, Schmidt-Grund R, Grundmann M. Raman tensor elements of β-Ga2O3. Sci Rep. 2016;6:35964

38. Sander T, Eisermann S, Meyer BK, Klar PJ. Raman tensor elements of wurtzite ZnO. Phys Rev B. 2012;85:165208

39. Strach T, Brunen J, Lederle B, Zegenhagen J, Cardona M. Determination of the phase difference between the Raman tensor elements of the A1g-like phonons in $SmBa_2Cu_3O_{7-\delta}$. Phys Rev B. 1998;57:1292-1297

Table I Raman tensors obtained via APR scattering spectrum and first-principle calculation.

Mode	Experimental	Calculated
A_g^1	/	$\begin{pmatrix} 0.064e^{i0.24\pi} & 0 & 0 \\ 0 & 0.025e^{i0.05\pi} & 0 \\ 0 & 0 & 0.033 \cdot e^{i0.01\pi} \end{pmatrix}$
	$a_1/c_1 = 3.33$	$a_1/c_1 = 1.94$
	$b_1/c_1 = 0.21$	$b_1/c_1 = 0.76$
	$\varphi_{a_1c_1} = 0.23\pi$	$\varphi_{a_1c_1} = 0.23\pi$
	$\varphi_{b_1c_1} = 0$	$\varphi_{b_1c_1} = 0.03\pi$
B_{2g}	/	$\begin{pmatrix} 0 & 0 & 0.08 \\ 0 & 0 & 0 \\ 0.08 & 0 & 0 \end{pmatrix}$
	d	$d = 0.08$
B_{3g}^1	/	$\begin{pmatrix} 0 & 0 & 0 \\ 0 & 0 & 0.03 \\ 0 & 0.03 & 0 \end{pmatrix}$
	f	$f = 0.03$
A_g^2	/	$\begin{pmatrix} 0.43e^{i0.29\pi} & 0 & 0 \\ 0 & 0.0045e^{i0.04\pi} & 0 \\ 0 & 0 & 0.28e^{i0.3\pi} \end{pmatrix}$
	$a_2/c_2 = 1.39$	$a_2/c_2 = 1.54$
	$b_2/c_2 = 0.45$	$b_2/c_2 = 0.016$
	$\varphi_{a_2c_2} = 0.44\pi$	$\varphi_{a_2c_2} = 0.01\pi$
	$\varphi_{b_2c_2} = 0.28\pi$	$\varphi_{b_2c_2} = 0.26\pi$

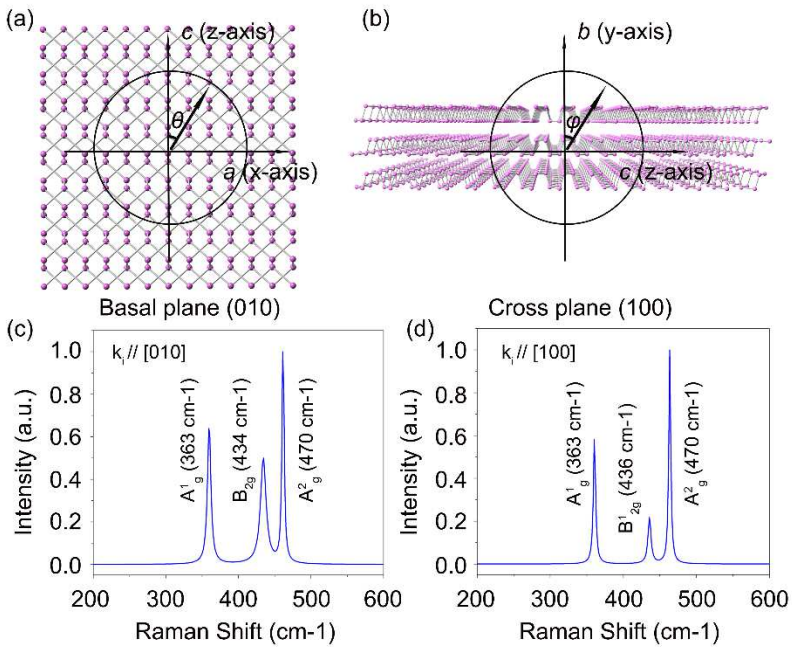

Fig. 1 Schematic of ARP Raman scattering of basal and cross plane of BP. (a) ARP Raman scattering of basal plane, θ is the angle between polarization direction of incident light and *c* axis. (b) APR scattering of cross plane, φ is the angle between polarization direction of incident light and *b* axis. (c) and (d) denote representative Raman spectra of basal and cross plane.

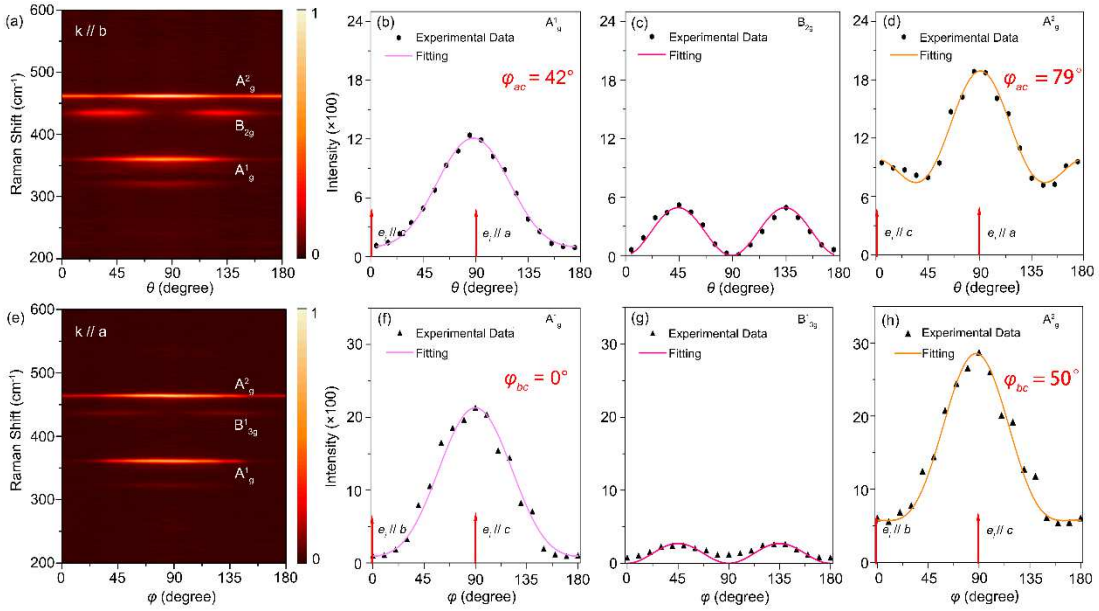

Fig. 2 ARP Raman scattering spectra of BP for (a)-(d) basal plane and (e)-(h) cross plane. ARP Raman scattering intensities were fitted with Eq. (4) and (6), and the phase differences between Raman tensor elements a and c ϕ_{ac} of A_g^1 and A_g^2 modes are 42° and 79° for basal plane. For cross plane, the phase differences between Raman tensor elements b and c of A_g^1 and A_g^2 modes are 0° and 50° respectively.

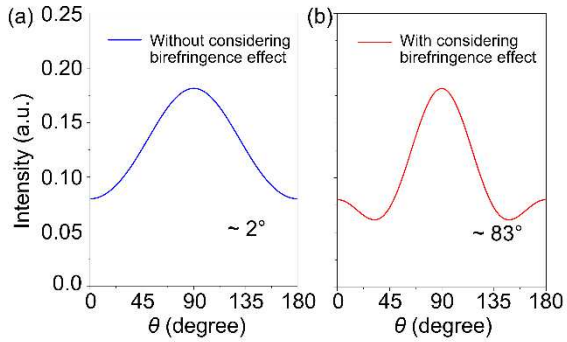

FIG. 3 Calculated basal plane APR spectrum of A_g^2 with and without considering birefringence effect.

Figures

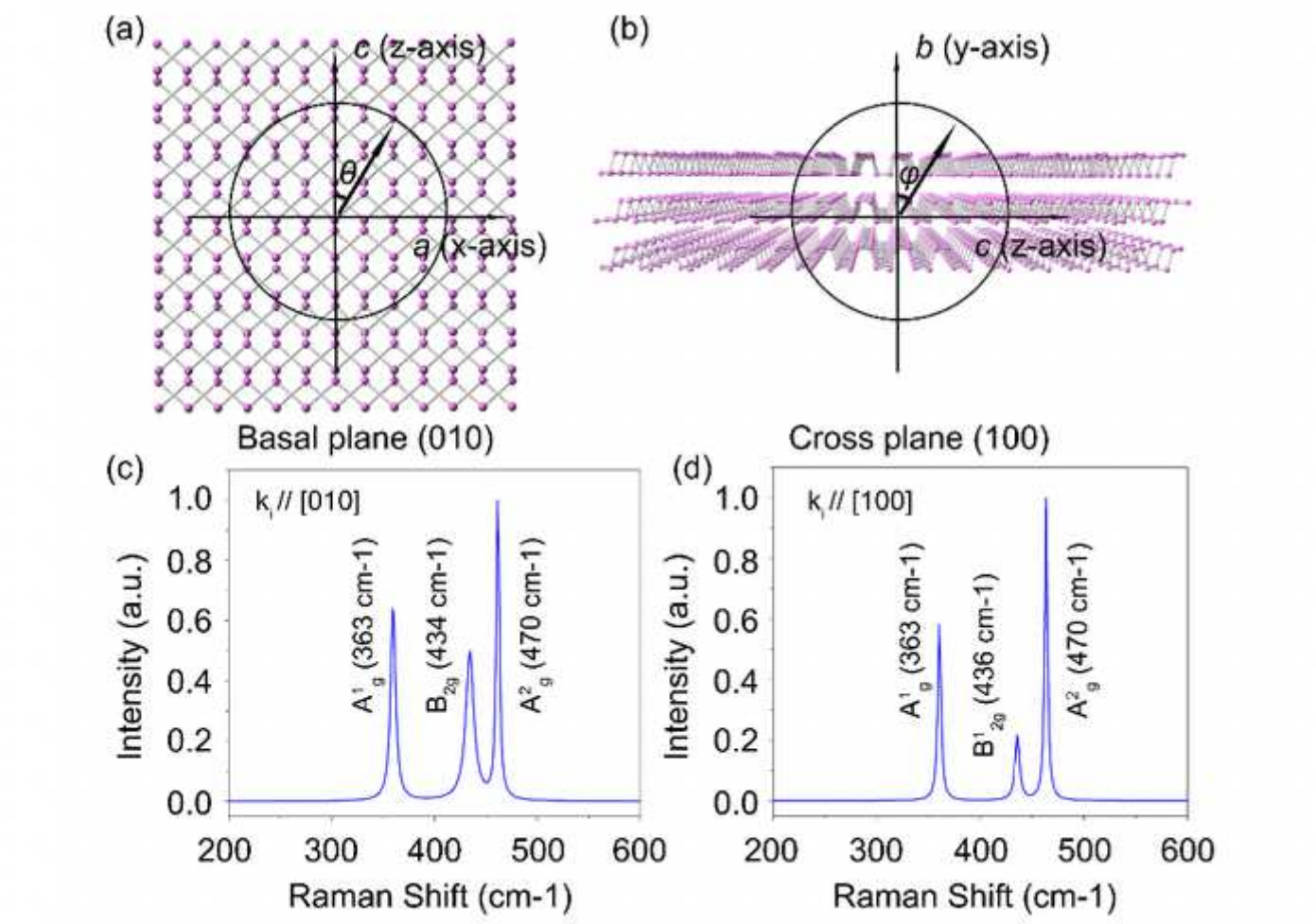

Figure 1

Schematic of ARP Raman scattering of basal and cross plane of BP. (a) ARP Raman scattering of basal plane, θ is the angle between polarization direction of incident light and c axis. (b) APR scattering of cross plane, φ is the angle between polarization direction of incident light and b axis. (c) and (d) denote representative Raman spectra of basal and cross plane.

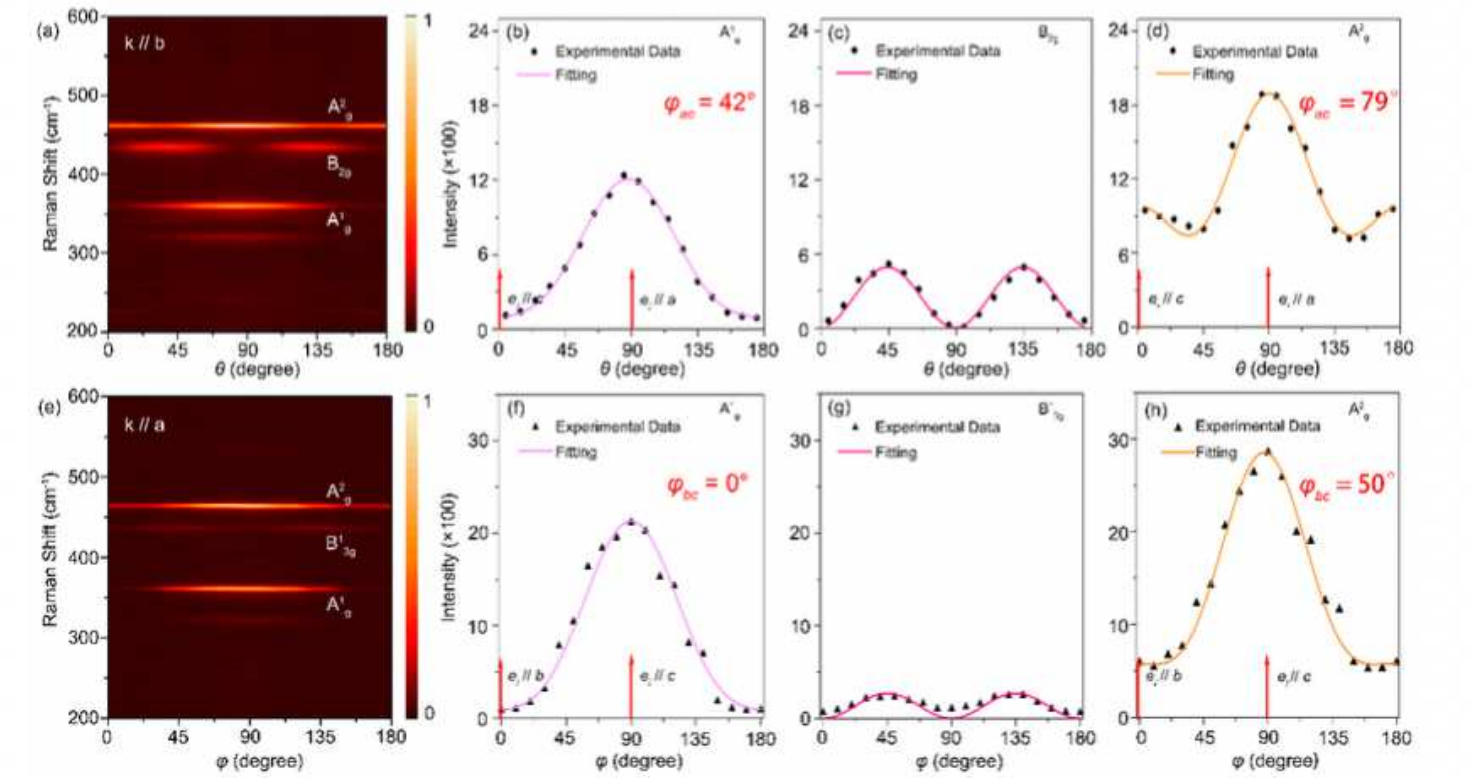

Figure 2

ARP Raman scattering spectra of BP for (a)-(d) basal plane and (e)-(h) cross plane. ARP Raman scattering intensities were fitted with Eq. (4) and (6), and the phase differences between Raman tensor elements a and c □_ac of A_g^1 and A_g^2 modes are 42° and 79° for basal plane. For cross plane, the phase differences between Raman tensor elements b and c of A_g^1 and A_g^2 modes are 0° and 50° respectively.

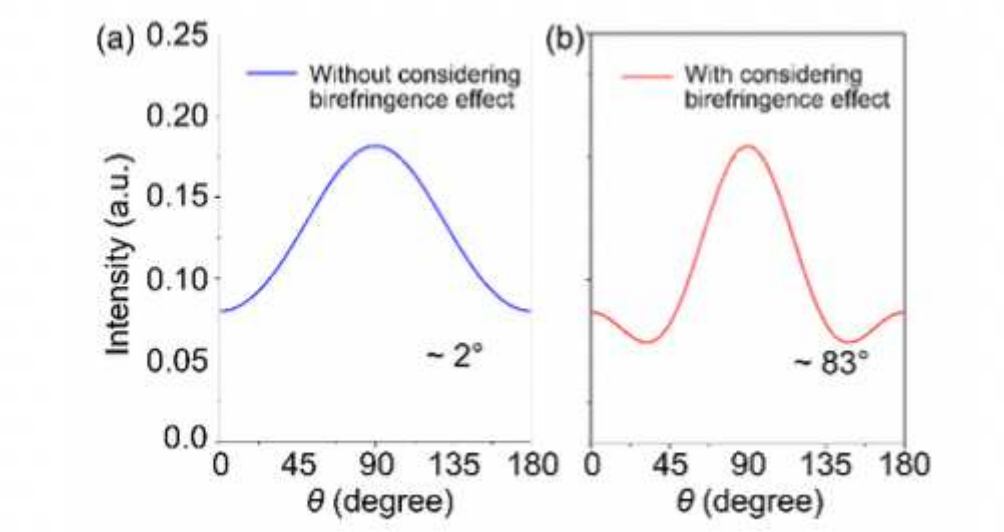

Figure 3

Calculated basal plane APR spectrum of A_g^2 with and without considering birefringence effect.

Supplementary Files

This is a list of supplementary files associated with this preprint. Click to download.

- SupplementaryInformation.pdf